Supplementary Information

Tailoring of highly-stable $Mn_{1-x-y}(Ce_xLa_y)O_{2-\delta}$ pseudocapacitor thin-film and rare earth oxide nanospheres through selective purification of rare earth oxides derived from Ni-MH batteries

Samane Maroufi*, Sajjad S. Mofarah§, Rasoul Khayyam Nekouei§,

and Veena Sahajwalla

1 *Centre for Sustainable Materials Research and Technology (SMaRT), School of Materials Science and Engineering, University of New South Wales, Sydney 2052, Australia*

*Corresponding author, Email: s.maroufi@unsw.edu.au

§ Authors have equal contributions.

Table of Contents

Our pr

1. Experimental Procedure

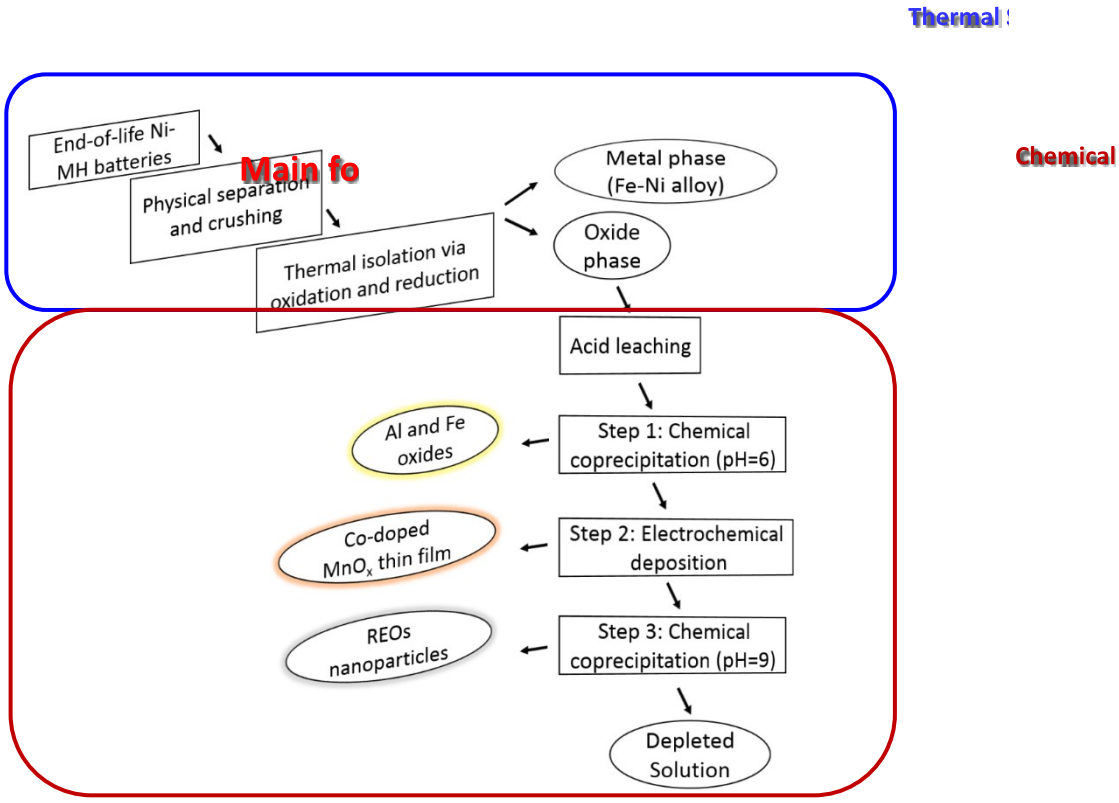

Figure S1. Flowchart of the selective thermal isolation-purification process, where the blue rectangles are the process described in Ref.[1], and the red rectangle is the process described in this manuscript.

Thermal isolation process

Spent Ni-MH batteries were dismantled manually. The plastic cases were manually separated, and the cell was cut longitudinally; the active components were separated from the plastic pieces. The dismantling of selected Ni-MH batteries exhibited two-electrode plaques separated via a polymer sheet impregnated by KOH electrolyte. The materials of the exterior housing were Ni-plated steel surrounded with a plastic case. The anode powder was separated from the supporting metal mesh and other parts. This powder was dried in an oven overnight and then analysed using X-ray diffraction (XRD, in **Fig. S2a**), X-ray fluorescence (XRF, in **Table S1**), and inductively coupled plasma (ICP) technique.

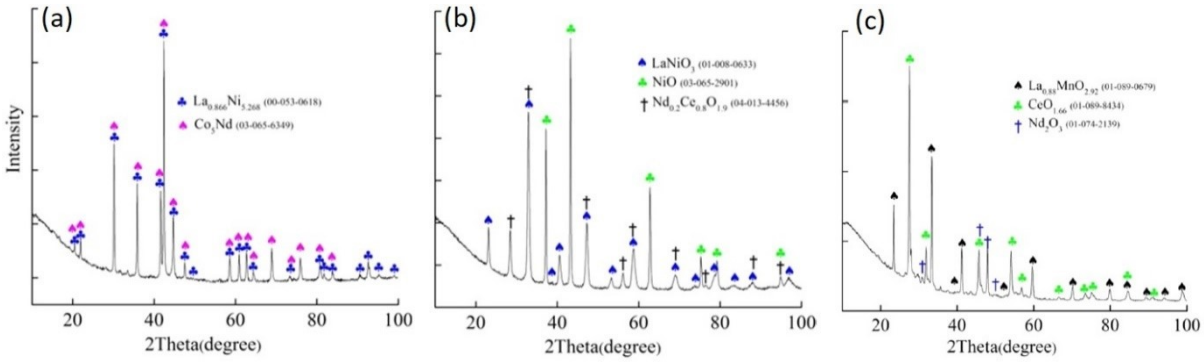

Figure S2. XRD patterns of **a)** as-received anode powder of Ni-MH battery, **b)** anode powder after oxidation at 1000°C for 1 h, and **c)** oxide phase rich in REOs separated after reduction-oxidation at 1550°C for 90 min; taken from Ref.[1].

Table S1. Composition of the anode powder of dismantles Ni-MH battery, taken by X-ray fluorescence (XRF) analysis.

element	Ni	La	Ce	Nd	Co	Mn	Al
Wt%	54.1	23.7	6.7	3.6	5.4	3.4	0.3

The embedded rare earth elements were thermally isolated in oxide form via an oxidation-reduction process. After exposure of the anode powder of dismantles Ni-MH battery (with the composition shown in **Table S1**) to an oxidation process in air at 1000°C for 1 h, the resulting oxide components (identified by XRD in **Fig. S1b** as $LaNiO_3$, NiO, and $Nd_{0.2}Ce_{0.8}O_{1.9}$)[1] were subjected to a reduction process (at 1550°C for 1.5 h) where waste iron was utilised as a reducing agent. Oxides of nickel and cobalt were reduced and diffused into metallic iron, resulting in the formation of ferronickel alloy and isolation of REEs in oxide phase (as shown in **Fig. S1c**) with a clear interface[1].

In terms of Mn, Mn is majorly accumulated in the metal phase after the reduction-oxidation stage at 1550°C; however, the minimal amount of left Mn needs to be removed to produce pure REOs. As mentioned in the text, Mn is regarded as a hard-to-remove impurity from REEs via precipitation (due to close precipitation pH), so the Mn removal can be only carried out via electrodeposition up to a few ppm.

Advanced characterisation equipment and parameters

The composition of the resulting phases was further analysed by X'pert PRO multi-purpose X-ray diffraction (XRD, MPD system) with Cu Kα wavelength and 2θ between 10-100°. The morphology of the sample was observed by field emission scanning electron microscopy (FE-SEM, NanoSEM 450 NOVA). Raman data were obtained by a Renishaw inVia Raman microscope (Gloucestershire, UK), which is equipped with a He-Ne green laser (λ = 514 nm) and diffraction grating of 1800 g/mm. Prior to characterisation, the equipment was calibrated against the silicon peak at ~520 cm^{-1}. The Raman spectra were obtained for the

range 100-800 cm^{-1}, and spot size ~4 µm. The data were analysed by Renishaw WiRE 4.4 software. Transmission electron microscopy (TEM, Philips CM200) equipped with energy dispersive spectroscopy (EDS, Bruker QUANTAX) was employed in measuring the interplanar spacing. Another TEM equipment (JEOL JEM-F200) with an elemental mapping resolution of 0.5 nm was employed as a scanning transmission electron microscope (STEM). To find out the chemical state or oxidation number of elements, X-ray photoelectron spectrometer (XPS, Thermo Scientific ESCALAB250i with monochromated Al Kα line (1486.68 eV) as the X-ray source) analysis was utilised under high vacuum (2^{-9} mbar) with 20 eV passing energy. The thickness and composition of the films were subjected to time-of-flight secondary ion mass spectroscopy (TOF-SIMS) under positive polarity by Bi_3^+ at 30 KeV and sputtered by Cs^+ beam of 1000 eV.

2. Results and Discussion

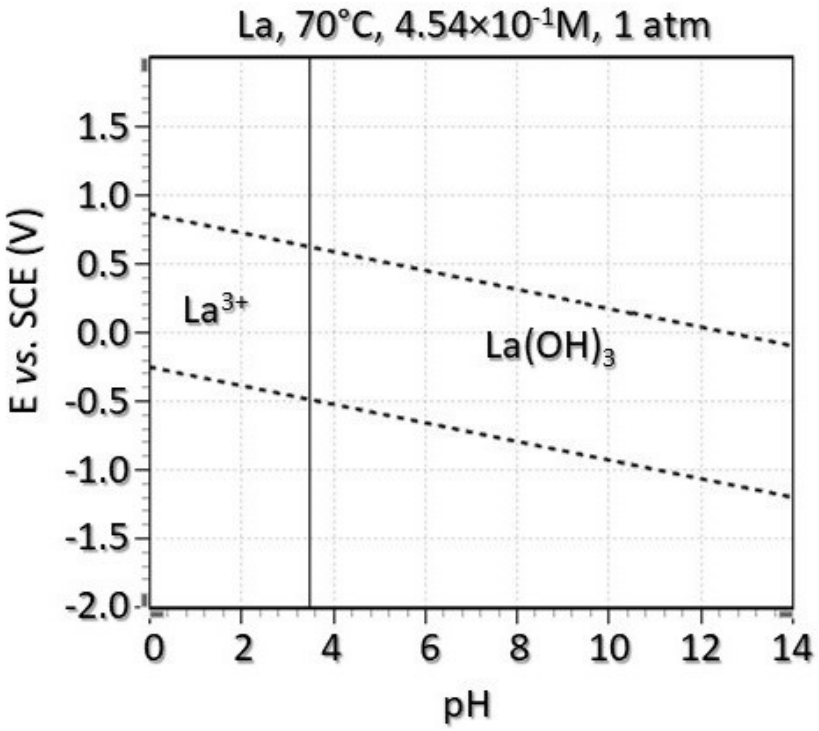

Figure S3. Pourbaix diagram for the minor element (*i.e.*, La) present in the electrodeposited film.

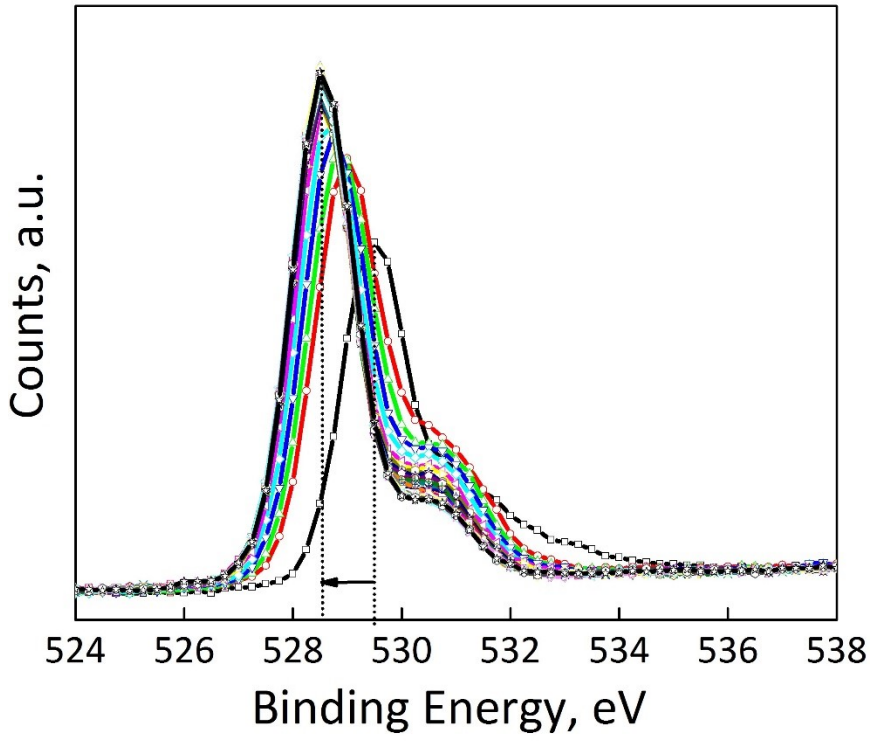

Figure S4. 2D XPS profile of O 1s at different depths from 1 to 312 nm for the $Ce^{4+/3+}$/La^{3+} co-doped MnO_{2-x}.

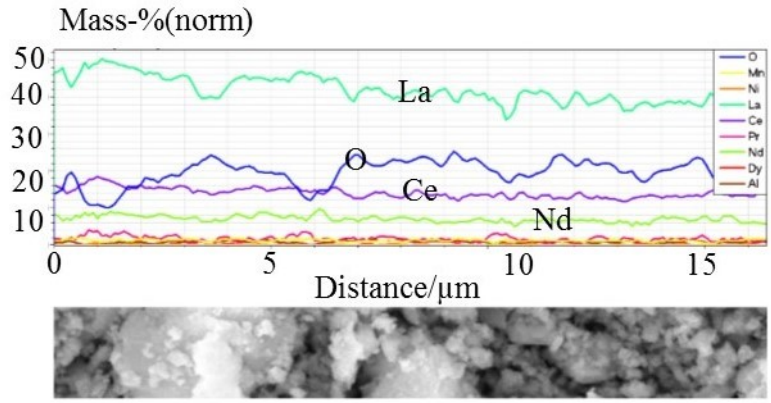

Figure S5. Elemental EDS line scan of the synthesised REO (La, Ce, Nd, and Pr) nanoparticles after thermal treatment at 700°C.

Table S2. Results of EDS point analysis of 5 different places from the synthesised REO (La, Ce, and Nd) nanoparticles.

Element (wt%)	P5	P4	P3	P2	P1	**Average (wt%)**	STD	Error (wt%)
La	43.05	42.66	40.48	38.86	38.71	**40.75**	2.05	1.3
O	32.97	29.31	33.50	35.87	36.52	**33.63**	2.85	4.26
Ce	17.45	14.88	13.63	13.45	13.40	**14.56**	1.72	0.48
Nd	2.39	8.68	7.83	7.58	7.29	**6.75**	2.49	0.27
Pr	2.16	2.17	2.31	2.01	1.96	**2.12**	0.14	0.11
Al	1.25	1.59	1.67	1.63	1.50	**1.53**	0.17	0.09
Si	0.71	0.71	0.59	0.58	0.62	**0.64**	0.06	0.06
Sum	100	100	100	100	100	**100**		

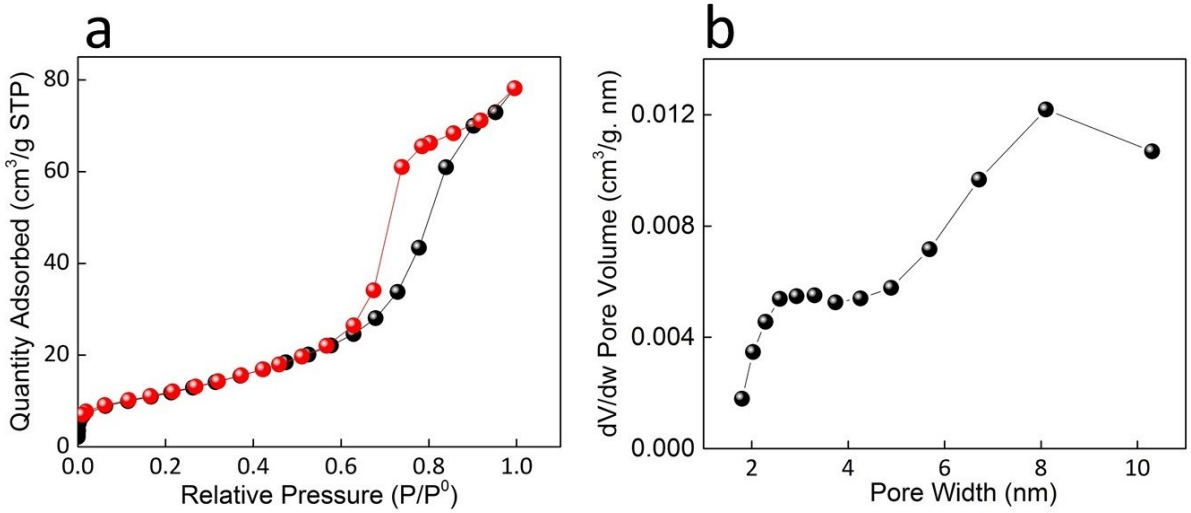

Figure S6. a) BET adsorption-desorption plot and **b)** pore width (by BJH method based on Gibbs adsorption behaviour) plots of REO nanoparticles.

Table S3. Details of the data extracted from BET analysis for REO nanoparticles.

Parameter	Value
Single point surface area at p/p° = 0.313972572	42.1 $m^2.g^{-1}$
BET Surface Area	42.1 $m^2.g^{-1}$
Langmuir Surface Area	138.3 $m^2.g^{-1}$
Adsorption average pore diameter (4V/A by BET)	10.7 nm
BJH Adsorption average pore width (4V/A)	6.5 nm
BJH Desorption average pore width (4V/A)	6.1 nm

Table S4. Overall comparative results of environmental impacts associated with the process of the synthesis of pure REO nanoparticles derived from end-of-life Ni-MH batteries versus their synthesis from virgin materials, i.e., pure REOs available in the market.

Impact category	Unit	Pure nanostructured REO sourced from NiMHB	Pure nanostructured REO from virgin resource
Ozone depletion	kg CFC-11 eq	2.12217E-08	4.74265E-08
Global warming	kg CO2 eq	0.278217095	0.346092952
Smog	kg O3 eq	0.012784492	0.016905651
Acidification	kg SO2 eq	0.001098897	0.001573721
Eutrophication	kg N eq	0.00034651	0.000711341
Carcinogenics	CTUh	5.69395E-09	1.50589E-08
Non-carcinogenics	CTUh	4.32433E-08	9.78241E-08
Respiratory effects	kg PM2.5 eq	0.000108258	0.0002198
Ecotoxicity	CTUe	1.093831679	2.365119075
Fossil fuel depletion	MJ surplus	0.200300872	0.446253599

3. References

1 S. Maroufi, R. K. Nekouei, R. Hossain, M. Assefi and V. Sahajwalla, *ACS Sustain. Chem. Eng.*, 2018, 6, 11811-11818.